Hydroxamate anchors for water-stable attachment to TiO_2 nanoparticles†

William R. McNamara, Robert C. Snoeberger III, Gonghu Li, Christiaan Richter, Laura J. Allen, Rebecca L. Milot, Charles A. Schmuttenmaer,* Robert H. Crabtree,* Gary W. Brudvig* and Victor S. Batista*

Received 26th May 2009, Accepted 31st July 2009
First published as an Advance Article on the web 7th August 2009
DOI: 10.1039/b910241h

Surface functionalization of nanoparticles is of broad interest, such as for dye attachment in dye-sensitized solar cells (DSSCs)[1,2] and photocatalysis.[3,4] Visible-light photoexcitation of the dye gives interfacial electron transfer (IET) into the conduction band of a semiconductor host.[5] In a Grätzel cell, TiO_2 is functionalized with Ru polypyridyl complexes that attach *via* carboxylate substituents[2] that permit ultrafast IET but are unstable in aqueous conditions.[6] We now report on hydroxamate anchors for robust TiO_2 functionalization even in aqueous conditions.

Hydroxamate ligands bind tightly to transition metals, even in water.[7,8] For example, bacterial siderophores that contain hydroxamates can dissolve Fe(III) from the oxide.[7] Recent studies have reported binding of hydroxamic acids to TiO_2.[8] Here, we investigate their potential as robust anchors for functionalization of TiO_2 thin-films commonly used in solar energy conversion and photocatalysis. We synthesize and deposit a hydroxamate-functionalized terpyridine and demonstrate visible-light sensitization of TiO_2 and activation of Mn adsorbates by ultrafast IET by using spectroscopy and molecular modeling.

The synthesis (Scheme 1) builds on prior methods[9] and proceeds in two steps in good yield. The methyl ester (**1**) reacts with *O*-Bn hydroxylamine ($BnONH_2$) in the presence of LiHMDS to give the corresponding ester.[10] The ester is then deprotected with H_2 and Pd/C to give the product **2**.

Degussa P25 TiO_2 nanoparticles (NPs) were sensitized with a solution of **2** in dry EtOH using known techniques.[4,11] The resulting sensitized nanoparticles were characterized using UV-visible and FTIR spectroscopy (see Fig. S1 and S2†). The spectroscopic data are consistent with **2** anchoring to TiO_2 *via* the hydroxamate. Upon binding, the disappearance of a C=O stretch at 1635 cm^{-1} present in the IR of unbound **2** is consistent with a $^{-}O–CR=N–O^{-}$ unit binding to TiO_2 with terpyridine pointing away from the surface, an arrangement that is particularly suitable for the subsequent immobilization of a metal for photocatalysis. We have immobilized Mn(II) by treating the **2**–TiO_2 assembly with 2 mM aq. $Mn^{II}(OAc)_2$.

Fig. 1a shows the characteristic EPR spectra at 6 K of a Mn(II) complex incorporated into **2**–TiO_2. In the dark, the Mn(II) signal is clearly visible (red) and, under illumination with visible light ($\lambda \geq 420$ nm), the Mn(II) signal decreases (blue) indicating Mn(II) photooxidation to Mn(III). After the light is turned off, the Mn(II) signal fully recovers, indicating reversible photoinduced charge separation. Fig. 1 (right) shows the reversible photooxidation of Mn(II) with a 44 s half-life for e^-/h^+ recombination, indicating slower charge recombination than for the analogous reaction with catechol or acetylacetonate anchors.[4,11] These results demonstrate visible-light oxidation of Mn(II) adsorbates through IET *via* the hydroxamate anchor into the TiO_2 conduction band.

To estimate the IET time scales and compare hydroxamate linkers to the corresponding carboxylate analogs, we simulated the IET dynamics in fully atomistic models of functionalized TiO_2 nanostructures, as previously reported,[4,11,12] according to mixed quantum-classical molecular dynamics. The simulations predict that both linkers lead to ultrafast, subpicosecond, IET rates and that hydroxamate anchors could replace carboxylates without altering the charge separation efficiency. Fig. 2 shows the survival probability for the electron to remain on the photoexcited adsorbate, along with a snapshot of the electronic charge distribution at 100 fs after photoexcitation: more than 50% of the electron charge is injected within the first 100 fs of dynamics.

With time resolved terahertz spectroscopy (TRTS) we have measured the time scale and efficiency of charge injection into TiO_2 NPs functionalized with **2** (Fig. 3). These measurements have subpicosecond temporal resolution and exploit the fact that mobile electrons absorb THz radiation when injected into the TiO_2 conduction band.[13] The THz transmission amplitude decreases when electrons are injected into the TiO_2 conduction band upon adsorbate photoexcitation. Fig. 3 shows the time dependent change in THz transmittance due to ultrafast interfacial electron injection induced by 400 nm photoexcitation of TiO_2 NP colloidal thin films

Broader context

Attachment of photoactive molecules to semiconductor TiO_2 nanoparticles is the basis of Grätzel dye-sensitized solar cells and of a number of proposed water-splitting solar cells. Many current linkers have either mediocre water-resistance or limited ability to transmit photoinjected electrons or are unstable to oxidative conditions. This paper demonstrates robust attachment *via* oxidation- and water-stable hydroxamate linkers that are also able to mediate photoinjection of electrons into TiO_2. Hydroxamates were selected because they have long attracted attention in a biological context—they are preferred ligands in siderophores where they bind tightly to Fe(III).

Department of Chemistry, Yale University, New Haven, Connecticut, 06520-8107. E-mail: charles.schmuttenmaer@yale.edu; robert.crabtree@yale.edu; gary.brudvig@yale.edu; victor.batista@yale.edu

† Electronic supplementary information (ESI) available: Synthesis, characterization, experimental procedures, and modeling. See DOI: 10.1039/b910241h

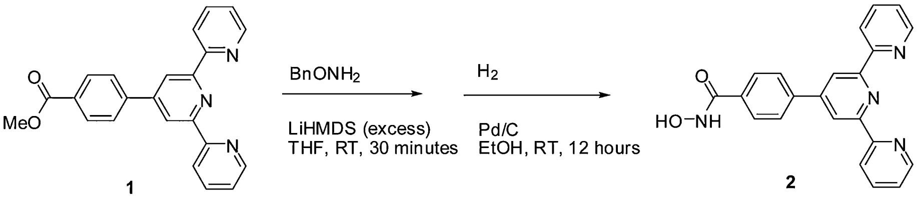

Scheme 1

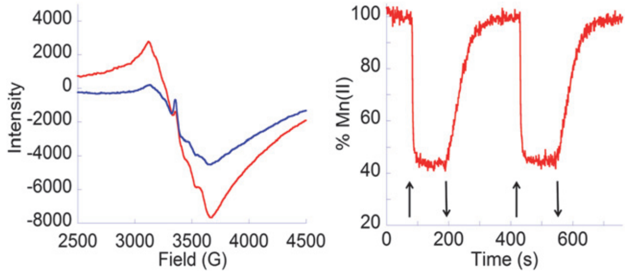

Fig. 1 *Left:* EPR spectra at 6 K of **2**–TiO$_2$ NPs functionalized with Mn^{II}(OAc)$_2$ in the dark before irradiation (▬) and with visible light irradiation (▬); *Right:* Time-dependent Mn(II) %age at 3106 G with light on (↑) and off (↓).

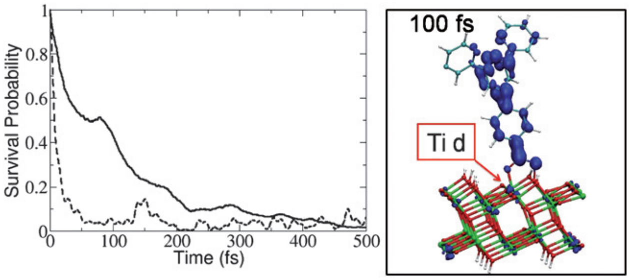

Fig. 2 *Left:* Time-dependent probability of the electron to remain in the adsorbate **2** (▬), compared to the analogous carboxylate-linked adsorbate (▪▪▪). *Right:* A snapshot of the electronic charge distribution at 100 fs after photoexcitation of **2**.

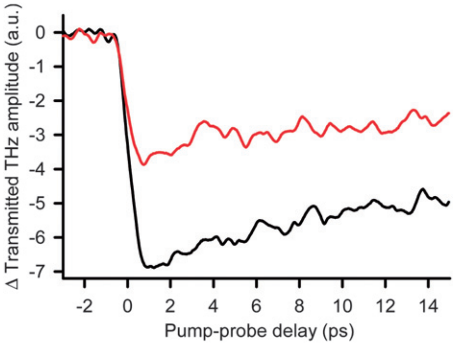

Fig. 3 400 nm pump/THz probe of electron injection in functionalized NP films of N719-TiO$_2$ (▬) and **2**-TiO$_2$ (▬).

functionalized with **2** (black) and the carboxylate-linked dye N719[2] (red). While the transmission unit in Fig. 3 is arbitrary, we have used the same scaling factor for both spectra to make meaningful amplitude comparisons between **2** and N719. The rapid decrease in THz transmission indicates that IET from the adsorbate to the NP is completed on a subpicosecond time scale after photoexcitation of the system. We note that the THz absorbance signal has a fast decay component that lasts ∼10 ps for both sensitizers and then levels off. This indicates that, within 10 ps, a fraction of the injected electrons either get trapped at TiO$_2$ defects or surface sites, or recombine with oxidized adsorbates. In addition, we have calculated the *apparent* injection efficiency of **2** relative to N719 with 400 nm excitation. Fig. 3 shows that 1.95 times as many electrons are injected with **2** relative to N719. At 400 nm, the absorbance of the sample functionalized with **2** is 0.67 and that for the N719 sample is 0.81 (Fig. S3†), and both films have the same thickness of 11.3 μm. The surface coverage is 1.20 and 0.99 molecules/nm^2 for **2** and N719, respectively (Table S1†). Therefore, given that there is a higher coverage of **2**, but a lower amount of absorbance, the fraction of molecules of **2** that have absorbed a photon is (0.99/1.20) × (0.67/0.81) = 0.68 times that of N719 (yet 1.95 times as many electrons are injected). Therefore, on a per molecule basis, **2** is 1.95/0.68, or 2.9 times more efficient than N719 for electron injection when exciting with 400 nm light. Since N719 is thought to be 100% efficient, this should not be taken to mean that we have an efficiency > 100%. The THz data only records mobile injected electrons and thus we only argue that hydroxamate is not inefficient for IET.

The stability of hydroxamate anchors has been compared to a carboxylate analogue *via* binding enthalpy calculations and UV-visible spectroscopic data. The calculations suggest that hydroxamates are *ca.* 33% more stable (∼10 kcal mol^{-1}) than carboxylates on TiO$_2$ anatase. Possible reasons are the dianionic charge, the less strained hydroxamate bite angle (∼75°) *versus* chelating carboxylate (∼61°) and the higher pK_as for hydroxamic acids (8.88 for MeCONHOH)[8a] *versus* carboxylic acids (4.76 for MeCOOH). Experimentally, hydroxamate anchors are more stable to water. Fig. 4 (left) compares the UV-visible spectrum of **2**–TiO$_2$ to that of bare TiO$_2$. The absorbance of **2**–TiO$_2$ at 420 nm likely corresponds to visible light excitation

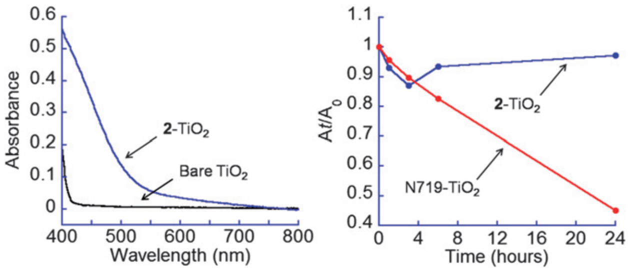

Fig. 4 *Left:* UV-visible spectra of **2**–TiO$_2$ (▬) and bare TiO$_2$ (▬). *Right:* Amounts of **2** and N719 remaining attached to TiO$_2$ NPs as a function of water incubation time from the absorbance A_t, at time t, relative to the A_0. The wavelengths used were 450 nm for **2**–TiO$_2$ and 550 nm for N719–TiO$_2$.

of an electron in the ligand HOMO to the conduction band of TiO_2. Fig. 4 (right) compares the absorption at 450 nm (blue trace, **2**–TiO_2) and 550 nm (red trace, N719–TiO_2) as a function of incubation time. Even after 24 h water exposure, there is no significant detachment of **2** (see also Fig. S3†). In contrast, the analogous experiment for N719 dye[2] shows a rapid decay of the absorbance.

The ease of synthesis, ability to induce ultrafast IET, and superior binding properties make hydroxamate anchors promising linkages for functionalizing TiO_2 thin-films suitable for DSSCs and photocatalysis and may lead to dye-sensitized solar cells that are more resistant to humidity.

Acknowledgements

We acknowledge support from the Chemical Sciences, Geosciences, and Biosciences Division, Office of Basic Energy Sciences, Office of Science, U.S. Department of Energy (DE-FG02-07ER15909) and DOE supercomputer time from NERSC. Also, NSF ECCS-0404191 grant supported preliminary work.

Notes and references

1 B. O'Regan and M. Grätzel, *Nature*, 1991, **353**, 737–740.

2 M. K. Nazeeruddin, A. Kay, I. Rodicio, R. Humphry-Baker, E. Muller, P. Liska, N. Vlachopoulos and M. Grätzel, *J. Am. Chem. Soc.*, 1993, **115**, 6382–6390.

3 (*a*) N. Serpone, *Res. Chem. Intermed.*, 1994, **20**, 953–992; (*b*) A. Mills and S. Leunte, *J. Photochem. Photobiol., A*, 1997, **108**, 1–35.

4 S. G. Abuabara, C. W. Cady, J. B. Baxter, C. A. Schmuttenmaer, R. H. Crabtree, G. W. Brudvig and V. S. Batista, *J. Phys. Chem. C*, 2007, **111**, 11982–11990.

5 (*a*) Y. X. Weng, Y. Q. Wang, J. , B. Asbury, H. N. Ghosh and T. Q. Lian, *J. Phys. Chem. B*, 2000, **104**, 93–104; (*b*) I. Martini, J. H. Hodak and G. V. Hartland, *J. Phys. Chem. B*, 1999, **103**, 9104–9111.

6 A. D. Weisz, A. E. Regazzoni and M. A. Blesa, *Solid State Ionics*, 2001, **143**, 125–130.

7 C. Cocozza, C. C. G. Tsao, S. F. Cheah, S. M. Kraemer, K. N. Raymond, T. M. Miano and G. Sposito, *Geochim. Cosmochim. Acta*, 2002, **66**, 431–438.

8 (*a*) J. Yang, P. J. Bremer, I. L. Lamont and A. J. McQuillan, *Langmuir*, 2006, **22**, 10109–10117; (*b*) H. G. Upritchard, J. Yang, P. J. Bremer, I. L. Lamont and A. J. McQuillan, *Langmuir*, 2007, **23**, 7189–7195.

9 (*a*) L. De Luca, G. Giacomelli and M. Taddei, *J. Org. Chem.*, 2001, **66**, 2534–2537; (*b*) M. P. Sibi, H. Hasegawa and S. R. Ghorpade, *Org. Lett.*, 2002, **4**, 3343–3346.

10 A. Gissot, A. Volonterio and M. Zanda, *J. Org. Chem.*, 2005, **70**, 6925–6928.

11 W. R. McNamara, R. C. Snoeberger, G. Li, J. M. Schleicher, C. W. Cady, M. Poyatos, C. A. Schmuttenmaer, R. H. Crabtree, G. W. Brudvig and V. S. Batista, *J. Am. Chem. Soc.*, 2008, **130**, 14329–14338.

12 (*a*) S. G. Abuabara, L. G. C. Rego and V. S. Batista, *J. Am. Chem. Soc.*, 2005, **127**, 18234–18242; (*b*) L. G. C. Rego, S. G. Abuabara and V. S. Batista, *J. Chem. Phys.*, 2005, **122**, 154709; (*c*) L. G. C. Rego and V. S. Batista, *J. Am. Chem. Soc.*, 2003, **125**, 7989–7997.

13 (*a*) J. B. Baxter and C. A. Schmuttenmaer, *J. Phys. Chem. B*, 2006, **110**, 25229–25239; (*b*) C. A. Schmuttenmaer, *Chem. Rev.*, 2004, **104**, 1759–1779.

Supporting Information for:

Hydroxamate Anchors for Water-Stable Attachment to TiO_2 Nanoparticles

William R. McNamara, Robert C. Snoeberger III, Gonghu Li, Christiaan Richter, Laura J. Allen, Rebecca L. Milot, Charles A. Schmuttenmaer,* Robert H. Crabtree,* Gary W. Brudvig,* and Victor S. Batista*
Yale University, Department of Chemistry, New Haven, Connecticut, 06520-8107.

April, 2009

This PDF file includes:
Methods and Models

- Synthesis and Characterization of **2.**
- Sample Preparation
- EPR Spectroscopy
- Surface Coverage Determination
- Time-Resolved Terahertz Spectroscopy Measurements
- Computational Procedures

Figures S1–S5.

- S1. Diffuse reflectance IR of **2** and **2**-TiO_2
- S2. UV-vis of **2**-TiO_2 and N719-TiO_2
- S3. UV-vis of water stability of **2**-TiO_2
- S4. ^1H NMR spectrum of **2**
- S5. ^{13}C NMR spectrum of **2**

I. Synthesis and Characterization of 2

1 was prepared by literature methods.[1] To a mixture of **1** (0.612 mmol) and $BnONH_2$ (0.612 mmol) in 15 mL of THF at room temperature, 3.1 eq of 1 M LiHMDS was added (1.90 mL, 1.90 mmol) dropwise. The solution was then stirred at room temperature for 30 minutes. The resulting yellow solution was quenched with the addition of saturated NH_4Cl and extracted 3 times with ethyl acetate. The combined organic layers were dried over magnesium sulfate, filtered, and the solvent removed under vacuum. The crude product was then dissolved in dry ethanol with Pd/C (10% by weight) and stirred at room temperature. To this mixture, 1 atm of $H_2(g)$ was added and stirred 12 hours at room temperature. The resulting solution was filtered through celite and the solvent was removed under vacuum. The resulting solid was suspended in hexanes, collected by vacuum filtration, and rinsed with additional hexanes to yield 0.289 mmol of **2** (47 % yield). ^1H NMR (CD_3OD, 400 MHz): δ 8.68-8.58 (m, 6H), 8.12-7.85 (m, 6H, CH_{AR}), 7.50 (t, 2H), 7.32-7.29 (s, 1H, NH), 4.57 (s, 1H, OH). ^{13}C NMR (CD_3OD, 500 MHz): δ158.93, 148.89, 148.55, 142.02, 141.62, 134.08, 130.27, 125.84, 120.53, 119.85, 117.03, 114.43, 111.29. Mass Spectroscopy: ES molecular ion calculated for $C_{22}H_{17}N_4O_2^+$: 369.1352; found m/z: 369.1346.

II. Sample Preparation

1. Sensitization of TiO_2 with **2**

Sensitized TiO_2 nanoparticles were prepared by stirring 30 mg of Degussa P25 TiO_2 nanoparticles (NPs) in 4 mL of a 0.9 mM solution of **2** in dry ethanol at room temperature for 12 hours. The resulting suspension was centrifuged to pellet the sensitized nanoparticles. The supernatant was then decanted, and the remaining pelleted particles rinsed with ethanol to obtain sensitized TiO_2 (denoted **2**-TiO_2).

The supplier of the N719 is EIC laboratories, Inc. The N719-TiO_2 NPs were prepared by stirring 15 mg of P25 in 60 mL of a 2 mM solution of N719 in ethanol at reflux for 12 h. The resulting nanoparticles were rinsed 3 times with ethanol, or until the ethanol remained colorless.

2. UV-visible Spectroscopic Measurements.

The samples for UV-visible spectroscopic measurements consist of thin mesoporous films (~10 μm thick) of Degussa P25 nanoparticles. The nanoparticles were doctor-bladed from aqueous solution onto a glass cover slip and annealed at 450 °C for 2 hours. The resulting slides were sensitized with **2** by stirring in dry ethanol at room temperature.[2] Films of P25 nanoparticles were highly scattering and spectra were obtained using a Varian Cary 3 spectrophotometer in diffuse reflectance geometry with an integrating sphere.

III. EPR Spectroscopy.

TiO_2 nanoparticles sensitized with $[Mn^{II}(H_2O)_3(\mathbf{2})]^{2+}$ were prepared by stirring **2**-TiO_2 with deionized H_2O and then soaking in a 2 mM aqueous solution of Mn(II) acetate for 2 hours. The resulting nanoparticles were washed with deionized H_2O, collected by centrifugation, and dried in the dark for EPR measurements. Perpendicular-mode EPR data were collected on an X-band Bruker Biospin/ELEXSYS E500 spectrometer equipped with a SHQ cavity and an Oxford ESR-900 liquid helium cryostat. All spectra were collected at 6 K on dry, powdered samples sealed in capillary tubes placed in 5 mm OD quartz EPR tubes containing 60/40 toluene/acetone which forms a transparent glass for efficient illumination of the sample and allows efficient heat transfer to prevent heating of the sample during illumination. Time-course measurements follow the signal intensity at 3106 G. All illuminations were carried out in the cryostat with white light passed through 420 nm long-pass and water filters. Relative Mn(II) concentrations are based on comparison of peak-to-peak amplitudes of both initial and illuminated signals at 3120 and 3667 G.

IV. Surface Coverage Determination

All samples were completely combusted in a Costech ECS 4010 elemental analyzer, and all N and C in the combustion products were quantified using a ThermoFinnigan DeltaPLUS Advantage mass spectrometer. The weight % of N is reported in Table S1. In addition, given that **2** has four N atoms and N719 has six, the wt. % can be converted to the number of moles of adsorbate per g of functionalized

---

* Corresponding Authors: robert.crabtree@yale.edu; gary.brudvig@yale.edu; victor.batista@yale.edu; charles.schmuttenmaer@yale.edu

TiO_2 NPs, which is then converted to a coverage in terms of molecules/nm^2 since it is well established that Degussa P25 has a specific surface area of 50 m^2/g.[3a] Thus, we find that the coverage of **2** is 1.20 molecules/nm^2, while that for N719 is 0.99 molecules/nm^2. Nazeeruddin et al.[3b] report a coverage of 1.3×10^{-7} mol/"projected cm^{2}" along with a roughness factor of ca. 1000 cm^2/"projected cm^{2}", allowing one to calculate a surface coverage of 1.3 µM/m^2, or 0.81 molecules/nm^2.

Table S1. % Nitrogen by weight for **2**-TiO_2 and N719-TiO_2 NPs. Values in parentheses are the 1 standard deviation uncertainties.

	2-TiO_2	N719-TiO_2
N (wt. %)	0.53844 ($1.3\cdot10^{-5}$)	0.66631 ($4.6\cdot10^{-3}$)
µM/g	96.107 ($2.3\cdot10^{-3}$)	79.285 ($5.4\cdot10^{-1}$)
molecules/nm^2	1.196 ($3\cdot10^{-5}$)	0.987 ($7\cdot10^{-3}$)

V. Time-Resolved Terahertz Spectroscopy Measurements.

An amplified Ti:sapphire laser (Tsunami/Spitfire from Spectra Physics) generating 800 mW of pulsed near-IR light at a 1 kHz repetition rate was used. The pulse width is ~100 fs and the center wavelength is 800 nm. Roughly 2/3 of the power is frequency doubled and then filtered to produce 50 mW of 400 nm light for the pump beam. The remainder of the near-IR light is used to generate and detect THz radiation using a 4-paraboloid arrangement that focuses the THz beam to a spot size of ~3 mm at the sample. Terahertz radiation is generated using optical rectification in a ZnTe(110) crystal and detected using free space electro-optic sampling in a second ZnTe(110) crystal. Terahertz data were taken at room temperature. The average of three samples was taken for each data set. Further information on the spectrometer and techniques has been reported in the literature.[4,5]

Terahertz radiation is adsorbed by mobile electrons in the TiO_2 conduction band and is insensitive to electrons within the absorbed sensitizer. A decrease in broadband THz (0.2 – 2 THz) transmission in photoexcited samples compared to non-photoexcited samples indicates a higher electron density in the TiO_2. Injection time is measured by monitoring the change in THz transmission as the delay time between the 400 nm pump and the THz probe is varied.

Given that the refractive index of the films is 2.47,[6] their thicknesses are determined by measuring the change in the arrival of THz waveforms transmitted through bare glass slides and transmitted through the same glass slide coated with the films. In each case, the additional delay due to the film was 55.4 ± 0.5 fs. Therefore, the film thickness is $\frac{55.4\text{ fs} \times 0.3\,\mu\text{m/fs}}{(2.47-1)} = 11.3\,\mu\text{m}$

VI. Computational Procedures.

To describe the attachment of **2** with TiO_2 nanoparticles, we used Density Functional Theory (DFT) calculations of the TiO_2 anatase (101) surface with the hydroxamate linker of **2** chelating a four-coordinate Ti^{4+} ion at an oxygen vacancy in the surface. The surface was represented by a slab, consisting of four layers of Ti^{4+} ions and eight layers of O^{2-} ions, that was periodically replicated in 3 dimensions. The dimensions of the slab were 10.49 Å x 15.18 Å x 5.9 Å in the [-101], [010] and [101] directions. A vacuum spacer of 10 Å was included to separate periodic slabs in the [101] direction.

The DFT calculations were performed using the plane-wave based Vienna Ab-initio Simulation Package (VASP).[7-9] Vanderbilt Ultrasoft pseudopotentials were used to describe the core electrons.[10] A 300 eV energy cutoff was used to truncate the plane-wave basis. Electron exchange and correlation were described using the PW91 generalized gradient approximation (GGA) functional. A 1 × 1 × 1 Monkhorst-Pack k-point sampling was used to integrate over the Brillouin zone. The geometry of the adsorbate and the six topmost layers of the TiO_2 slab were relaxed to the minimum energy configuration.

The binding enthalpies of hydroxamate anchors were estimated using benzohydroxamic acid as a model compound. The binding enthalpies were calculated by subtracting the energy of the clean surface and adsorbate in vacuum from the energy of the total system, adsorbate bound to the surface. The calculations predict that hydroxamate anchors bind 5 kcal/mol more strongly to the anatase (101) surface than benzoic acid, with an additional 5 kcal/mol of stabilization gained by dissociation of the nitrogen proton to a surface O^{2-} ion.

Simulations of IET were performed using the relaxed **2**-TiO_2 slab extended 3 × 3 in the [-101] and [010] directions. The electronic structure of the complete model system was obtained using the extended Hückel method. The initial state of the electron was prepared by projecting the LUMO of **2** into the molecular orbitals of the complete model system. The goal of our simulation was not to model electron relaxation after a π-π* excitation of **2**, which occurs in the UV, but after a MLCT to the LUMO of **2** from a metal center immobilized in the terpyridine.

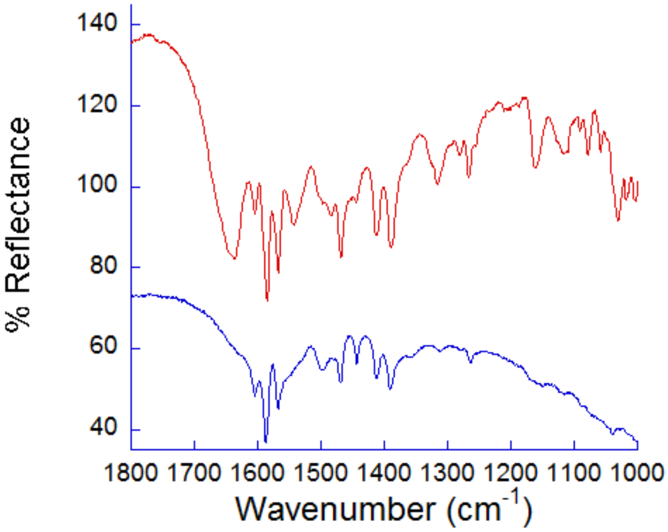

Figure S1. Diffuse Reflectance IR spectra of unbound **2** (red) and **2**-TiO_2 (blue).

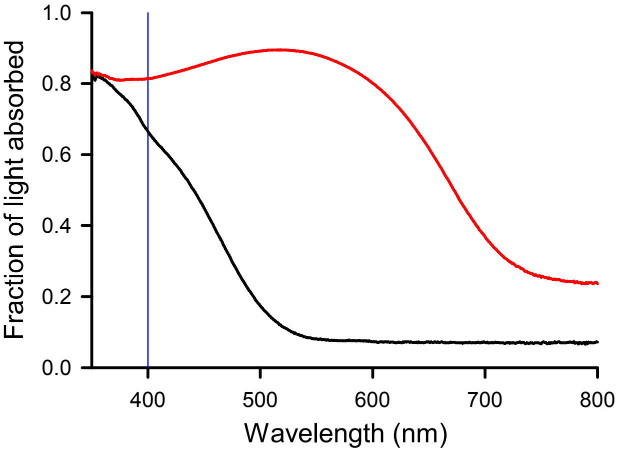

Figure S2. UV-visible spectra of **2**-TiO_2 (black) and N719-TiO_2 (red). The thin blue line represents the excitation wavelength of 400 nm.

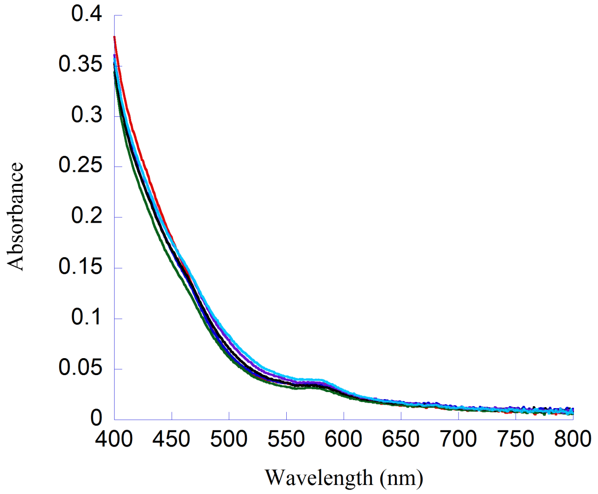

Figure S3. UV-visible spectra of **2**-TiO_2 after incubation in water for 0 hours (red), 1 hour (blue), 3 hours (green), 6 hours (black), 12 hours (purple), and 24 hours (light blue).

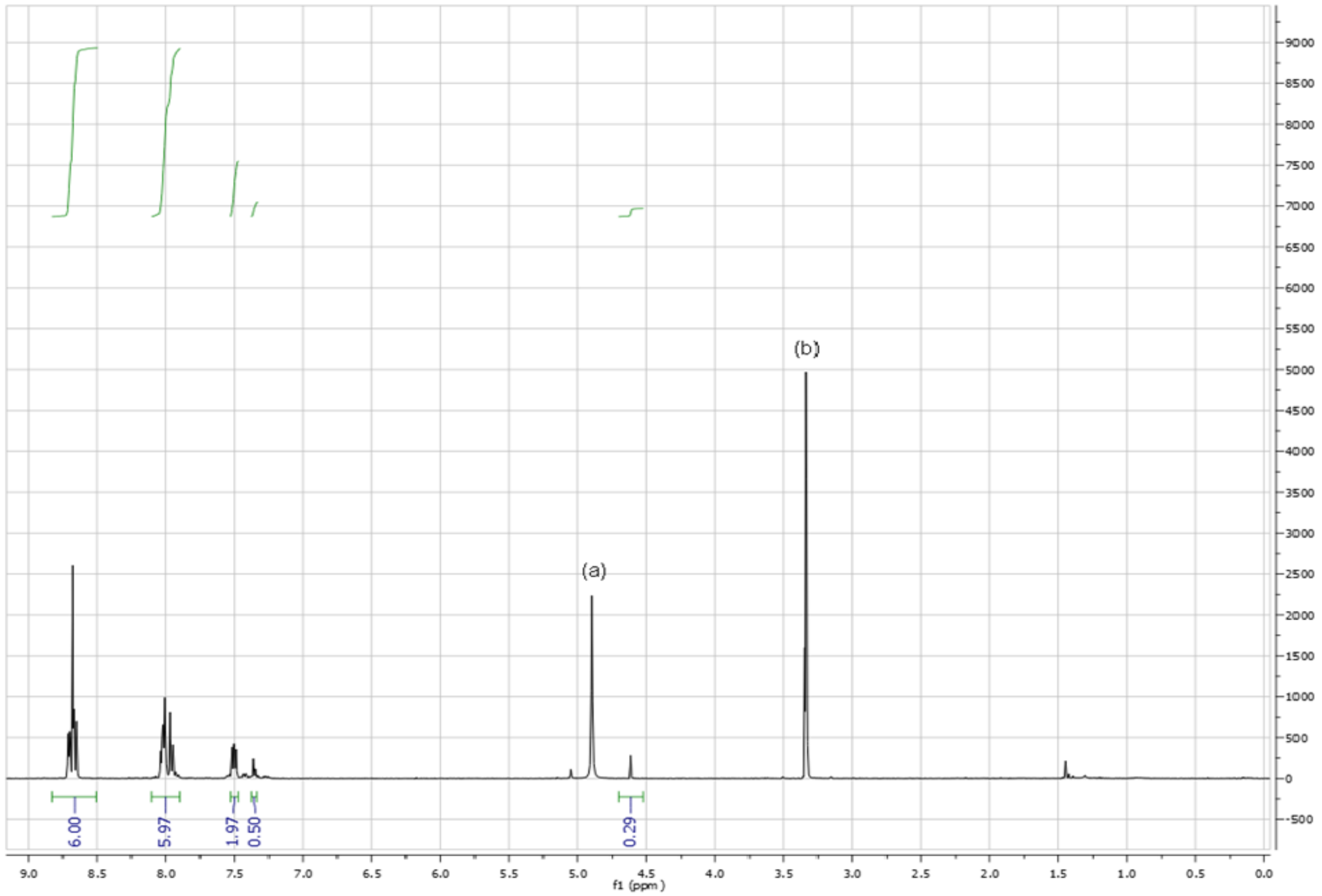

Figure S4. ^{1}H NMR spectrum of **2** in CD_3OD. Solvent residual peaks are noted at δ 4.87 (a), and 3.34 ppm (b) for water and methanol in CD_3OD, respectively.

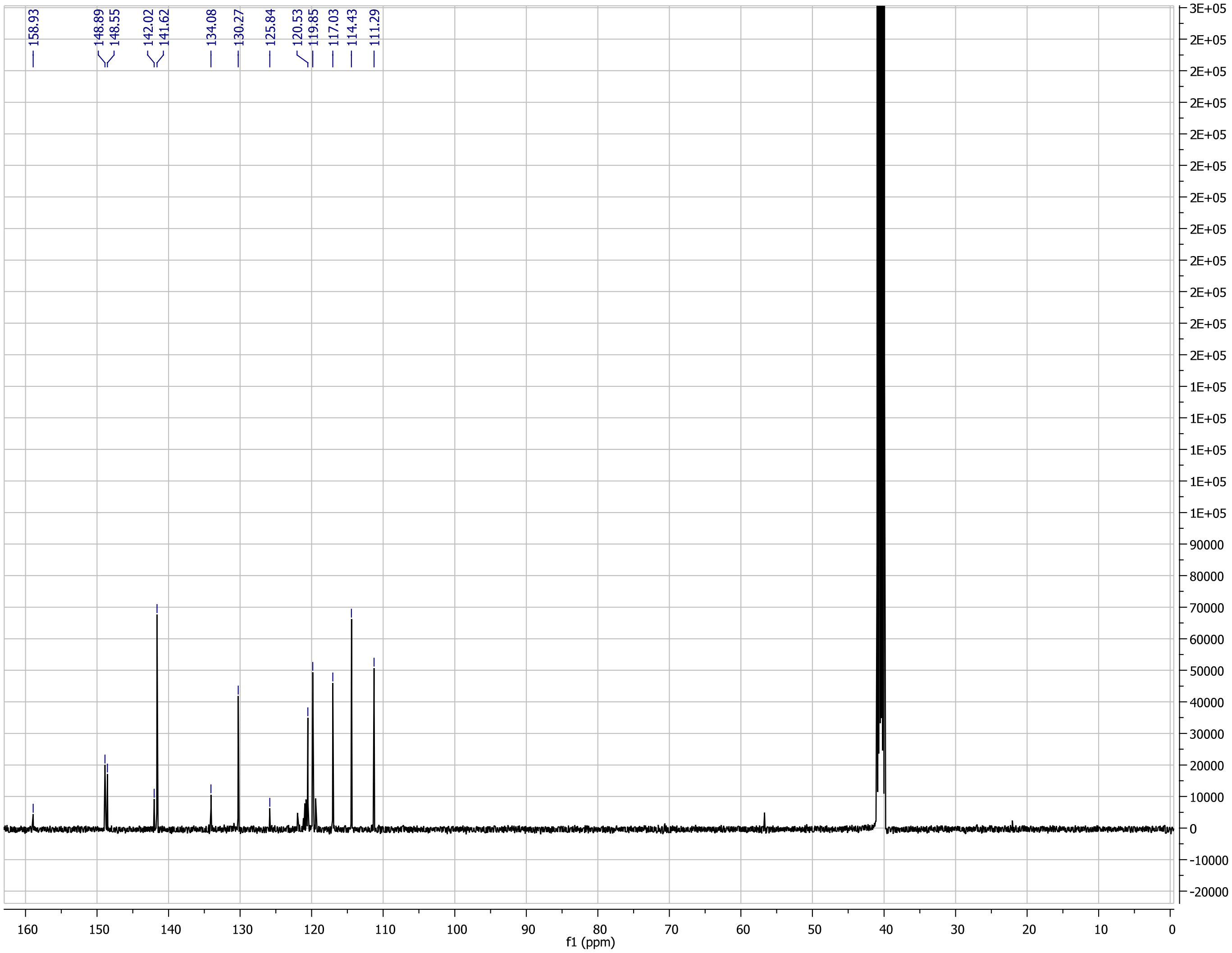

Figure S5. ^{13}C NMR spectrum of **2** in $(CD_3)_2SO$**.** A solvent residual peak is at δ40.45 ppm for $(CD_3)_2SO$.

References

(1) Wolpher, H.; Sinha, S.; Pan, J. X.; Johansson, A.; Lundqvist, M. J.; Persson, P.; Lomoth, R.; Bergquist, J.; Sun, L. C.; Sundstrom, V.; Akermark, B.; Polivka, T., "Synthesis and electron transfer studies of ruthenium-terpyridine-based dyads attached to nanostructured TiO$_2$," *Inorg. Chem.* **2007**, *46*, 638-651.

(2) McNamara, W. R.; Snoeberger, R. C.; Li, G.; Schleicher, J. M.; Cady, C. W.; Poyatos, M.; Schmuttenmaer, C. A.; Crabtree, R. H.; Brudvig, G. W.; Batista, V. S., "Acetylacetonate Anchors for Robust Functionalization of TiO$_2$ Nanoparticles with Mn(II)-Terpyridine Complexes," *J. Am. Chem. Soc.* **2008**, *130*, 14329-14338.

(3)(a) Li, G.; Sproviero, E. M.; Snoeberger, R. C.; Iguchi, N.; Blakemore, J. D.; Crabtree, R. H.; Brudvig, G. W.; Batista, V. S. *Energy Environ. Sci.* **2009**, 2, 230.

(b) Nazeeruddin, M. K.; Kay, A.; Rodicio, I.; Humphrybaker, R.; Muller, E.; Liska, P.; Vlachopoulos, N.; Grätzel, M., "Conversion of light to electricity by cis-X$_2$bis(2,2'-bipyridyl-4,4'-dicarboxylate)ruthenium(II) charge-transfer sensitizers (X = Cl$^-$, Br$^-$, I$^-$, CN$^-$, and SCN$^-$) on nanocrystalline TiO$_2$ electrodes," *J. Am. Chem. Soc.* **1993**, *115*, 6382-6390.

(4) Baxter, J. B.; Schmuttenmaer, C. A., "Conductivity of ZnO nanowires, nanoparticles, and thin films using time-resolved terahertz spectroscopy," *J. Phys. Chem. B* **2006**, *110*, 25229-25239.

(5) Beard, M. C.; Turner, G. M.; Schmuttenmaer, C. A., "Transient photoconductivity in GaAs as measured by time-resolved terahertz spectroscopy," *Phys. Rev. B* **2000**, *62*, 15764-15777.

(6) Turner, G. M.; Beard, M. C.; Schmuttenmaer, C. A., "Carrier localization and cooling in dye-sensitized nanocrystalline titanium dioxide," *J. Phys. Chem. B* **2002**, *106*, 11716-11719.

(7) G. Kresse, G.; Hafner, J. *Phys. Rev. B* **1993**, 47, 558; ibid. 1994, 49, 14251.

(8) Kresse, G.; Furthmuller, J. *Comput. Mat. Sci.* **1996** 6, 15.

(9) Kresse, G.; Furthmuller, J. *Phys. Rev. B* **1996**, 54, 11169.

(10) Kresse, G.; Hafner, J. *J. Phys.: Condens. Matt.* **1994,** 6, 8245.